# Murine coronavirus ubiquitin-like domain is important for papain-like protease stability and viral pathogenesis

**Anna M. Mielech[1], Xufang Deng[1], Yafang Chen[2], Eveline Kindler[3,4], Dorthea L. Wheeler[5], Andrew D. Mesecar[2], Volker Thiel[3,4], Stanley Perlman[5,6] and Susan C. Baker[1]**

[1]Department of Microbiology & Immunology, Loyola University Chicago Stritch School of Medicine, Maywood, IL, USA

[2]Purdue University, Department of Biological Sciences, USA

[3]Federal Institute of Virology and Immunology, Bern and Mittelhäusern, Switzerland

[4]Vetsuisse Faculty, University of Bern, Bern, Switzerland

[5]Interdisciplinary Program in Immunology, University of Iowa, Iowa City, IA, USA

[6]Department of Microbiology, University of Iowa, Iowa City, IA, USA

To whom correspondence should be addressed: sbaker1@luc.edu

**Running title**: ubiquitin-like domain stabilizes papain-like protease

**Word count** abstract: 250, importance 122, text 5195

**Abstract**

Ubiquitin-like domains (Ubls) are now recognized as common elements adjacent to viral and cellular proteases; however, their function is unclear. Structural studies of the papain-like protease (PLP) domains of coronaviruses (CoVs) revealed an adjacent Ubl domain in Severe Acute Respiratory Syndrome CoV, Middle East Respiratory Syndrome CoV, and the murine CoV, mouse hepatitis virus (MHV). Here we tested the effect of altering the Ubl adjacent to PLP2 of MHV on enzyme activity, viral replication and pathogenesis. Using deletion and substitution approaches, we identified sites within the Ubl domain, residues 785-787 of nonstructural protein 3, which negatively affect protease activity, and valine residues 785 and 787, which negatively affect deubiquitinating activity. Using reverse genetics, we engineered Ubl-mutant viruses and found that AM2 (V787S) and AM3 (V785S) viruses replicate efficiently at 37°C, but generate smaller plaques than WT virus, and AM2 is defective for replication at higher temperatures. To evaluate the effect of the mutation on protease activity, we purified WT and Ubl-mutant PLP2 and found that the proteases exhibit similar specific activities at 25°C. However, the thermal stability of the Ubl-mutant PLP2 was significantly reduced at 30°C thereby reducing the total enzymatic activity. To determine if the destabilizing mutation affects viral pathogenesis, we infected C57BL/6 mice with WT or AM2 and found that the mutant virus is highly attenuated, yet replicates sufficiently to elicit protective immunity. These studies revealed that modulating the Ubl domain adjacent to the PLP reduces protease stability and viral pathogenesis, revealing a novel approach to coronavirus attenuation.

47 **Importance**

48 Introducing mutations into a protein or virus can have either direct or indirect effects on
49 function. We asked if changes in the Ubl domain, a conserved domain adjacent to the
50 coronavirus papain-like protease, altered the viral protease activity or affected viral replication or
51 pathogenesis. Our studies using purified wild-type and Ubl-mutant proteases revealed that
52 mutations in the viral Ubl domain destabilize and inactivate the adjacent viral protease.
53 Furthermore, we show that a CoV encoding the mutant Ubl domain is unable to replicate at high
54 temperature or cause lethal disease in mice. Our results identify the coronavirus Ubl domain as a
55 novel modulator of viral protease stability and reveal manipulating the Ubl domain as a new
56 approach for attenuating coronavirus replication and pathogenesis.

57

58 **Introduction**

59 Coronaviruses are emerging human pathogens. Severe Acute Respiratory Syndrome
60 Coronavirus (SARS-CoV) caused the epidemic of 2002-2003, with ~10% case-fatality ratio (1).
61 Middle East Respiratory Syndrome Coronavirus (MERS-CoV) is a pathogenic virus that was
62 first identified in humans in 2012 (2). As of February 3, 2015 there have been 965 confirmed
63 cases and 357 deaths (3). For SARS-CoV, the virus emerged from a reservoir in bats, replicated
64 in an intermediate host (civet cats), and spread to humans. The epidemic strain of SARS-CoV
65 evolved for efficient human-to-human spread (4–6). Public health measures of isolation of
66 infected individuals led to the cessation of the epidemic in humans; however, SARS-like viruses
67 remain in bat reservoirs (7–9). For MERS-CoV, dromedary camels are now suspected as the
68 likely zoonotic source for transmission to humans since MERS-CoV sequences with 99%
69 nucleotide identity to human MERS-CoV isolates have been detected in respiratory samples

from camels (10). Although there are reports of human-to-human transmission of MERS-CoV (11, 12), current strains seem to cause mostly lower respiratory tract disease and are not as highly transmissible as SARS-CoV (13). Other human coronaviruses (HCoV-229E, HCoV-OC43, HCoV-NL63, HCoV-HKU1) are endemic in the human population and are the causative agents of upper and lower respiratory tract disease and croup (14–17). To date, there are no FDA approved antiviral drugs or vaccines to fight human coronavirus-induced disease. In addition, the potential exists for coronaviruses to emerge into the human population from endemic reservoirs in bats or other animals (18). Identifying viral components critical for efficient replication and manifestation of disease will facilitate antiviral drug and vaccine development.

Coronaviruses are RNA viruses that encode a replicase polyprotein at the 5'-end of the positive-strand genome. Upon virus entry, the genomic RNA is translated to produce replicase polyproteins (pp1a and pp1ab), which are processed by virally-encoded proteases. Depending on the virus species, the pp1a encodes one or two papain-like proteases (PLPs) and one 3C-like proteinase (3CLpro or Mpro). These proteases process the replicase polyproteins into non-structural proteins (nsps) that assemble with cellular membranes and facilitate virus replication (reviewed in (19)). Mouse hepatitis virus (MHV), the murine coronavirus used in this report, is commonly used as a model system to study the replication and pathogenesis of coronaviruses (20).

The MHV replicase product nsp3 consists of multiple domains including two PLP domains (PLP1 and PLP2), two predicted ubiquitin-like domains (Ubl), an acidic region (Ac), ADP-ribose-1"-phosphatase (ADRP), nucleic acid-binding domain (NAB), coronavirus group 2 marker domain (G2M), transmembrane segment (TM) and coronavirus highly conserved domain (Y) (reviewed in (21), shown in Fig. 1A). The Ubl-1 domain has been shown to interact with

93 nucleocapsid (N) protein, which is important for virus replication (21, 22). Previous studies
94 revealed that MHV PLP1 activity is required for processing the polyprotein at the nsp1/nsp2 and
95 nsp2/nsp3 sites (23). Further, the catalytic activity of PLP1 is required for efficient virus
96 replication (24). PLP2 was shown to recognize and process a LXGG motif and cleave the
97 replicase polyprotein at the nsp3/nsp4 junction (25). The LXGG recognition site is similar to the
98 RLRGG recognition site of cellular deubiquitinating enzymes. Lindner et al., 2005 was the first
99 to predict that CoV PLPs could be multifunctional enzymes with both protease and
100 deubiquitinating (DUB) activity (26). Indeed, further studies revealed that SARS-CoV PLpro,
101 MERS-CoV PLpro, HCoV-NL63 PLP2, PEDV PLP2 and MHV PLP2 are multifunctional
102 enzymes exhibiting protease, DUB and deISGylating (ability to deconjugate interferon
103 stimulated gene 15 protein, ISG15 from substrates (27–34)) activities. CoV PLP activity is
104 required for processing the replicase polyprotein and predicted to modulate the innate immune
105 response by deubiquitination of signaling molecules activated by pattern recognition receptors
106 such as RIG-I and MDA5 (29, 31, 35, 36). Structural studies of the papain-like protease domain
107 of SARS-CoV (37, 38) and more recently of MERS-CoV (39) and MHV (Chen et al., in
108 preparation), show that these enzymes belong to the ubiquitin-specific proteins (USP) family of
109 deubiquitinating enzymes and reveal the presence of a ubiquitin-like domain (Ubl) located
110 upstream of the protease domain (38). However, the role of the Ubl domain in modulating the
111 enzyme activity of MHV PLP2 is unknown.

112 Here, we investigated the role of the Ubl domain (designated Ubl-2) adjacent to PLP2 for
113 its function in MHV replication and pathogenesis. We generated proteases and viruses
114 containing mutations within the Ubl domain and found that these mutations decreased PLP2
115 activity and stability. Further, we found that these mutations resulted in decreased virus

116 replication and a marked attenuation of virulence. Immunization with the Ubl mutant virus
117 protected mice against challenge with wild-type virus. Overall, our data demonstrate for the first
118 time that manipulation of the Ubl domain adjacent to a viral protease can ameliorate viral
119 pathogenicity *in vivo*.
120
121 **Materials and methods**

122 **Cells.** HEK293T cells were cultured in Dulbecco's Modified Eagle Medium (DMEM) with 10%
123 fetal bovine serum (FBS) and 2% L-glutamine. DBT cells were cultured in Minimal Essential
124 Medium with 5% FBS, 2% L-glutamine, and 10% Tryptose Phosphate Broth (TPB). BHK-R
125 cells were kindly provided by Mark Denison (Vanderbilt University Medical Center) and
126 maintained in DMEM media supplemented with 10% FBS, 2% L-glutamine, and 0.8mg/ml
127 G418.

128 **Plasmids and mutagenesis**. PLP2 (amino acids 1525-1911) sequence in frame with a V5
129 epitope tag was codon-optimized and synthesized by Gene Script (Piscataway, NJ) (sequence
130 available upon request). Codon-optimized synthetic PLP2 sequence was cloned into pCAGGS-
131 MCS vector. For mutagenesis, an overlapping PCR strategy was used with primers described in
132 Table 1. The introduced mutations were verified by sequencing. The nsp2/3-GFP expression
133 plasmid was kindly provided Ralph Baric (University of North Carolina). The Flag-Ub plasmid
134 was kindly provided by Adriano Marchese (Loyola University Chicago).

135 **Protease and Deubiquitinase (DUB) Activity Assays.** To determine catalytic activity of the
136 PLP2 constructs, 70% confluent HEK293T cells in 12-well CellBIND plates (Corning) were
137 transfected using *Trans*IT-LT1 Reagent (Mirus) according to the manufacturer's protocol. For

the protease assay, the cells were transfected with 25ng nsp2/3-GFP plasmid and 300ng pCAGGS-PLP2-V5 expression plasmids (wild-type and various PLP2 mutants). To assess DUB activity the cells were transfected with 600ng Flag-Ub plasmid, and pCAGGS-PLP2-V5 expression plasmids (wild-type and various PLP2 mutants). At 24 hours post-transfection cells were lysed with 300µL of lysis buffer A containing 4% SDS and 3% dithiothreitol (DTT). Proteins were separated by SDS-PAGE and transferred to PVDF membrane in transfer buffer (0.025M Tris, 0.192M glycine, 20% methanol) for 1 h at 55V at 4°C. Following this, the membrane was blocked using 5% dried skim milk in TBST buffer (0.9% NaCl, 10mM Tris-HCl, pH7.5, 0.1% Tween 20) overnight at 4°C. The membrane was incubated with polyclonal rabbit anti-GFP antibody (Life Technologies) at a dilution of 1:2000 for the protease assay, or mouse anti-flag (Sigma) at the dilution of 1:2000 for the DUB assay. The membrane was washed 3 times for 15 minutes in TBST buffer followed by incubation with secondary donkey-anti-rabbit-HRP antibody at a dilution of 1:2000 (Amersham) for protease assay, or goat anti-mouse-HRP antibody at a dilution of 1:5000 (Amersham). Then the membrane was washed 3 times for 15 minutes in TBST buffer. Detection was performed using Western Lighting Chemiluminescence Reagent Plus (PerkinElmer) and visualized using a FluoroChemE Imager (Protein Simple). To verify expression of the PLP2 constructs, membranes were probed with mouse anti-V5 (Life Technologies) antibody at the dilution 1:5000. Mouse anti-calnexin (Cell Signal) antibody at a dilution 1:2000 was used as a loading standard.

**Biosensor Live Cell Assay.** To determine protease activity of the Ubl mutants, the previously described protocol was used (40). Briefly, HEK293T were transfected with 37.5ng pGlo-RLKGG construct and 50ng of PLP2 expression plasmids. At 18 hours post-transfection,



Journal of Virology

GloSensor (Promega) reagent diluted 1:50 in DMEM (10% FBS) was added. The luminescence was measured using a luminometer (Veritas) every hour for 5 hours.

**Generating Ubl-2 mutant viruses.** To introduce mutations into MHV A59, we used a previously described method (40). Briefly, plasmid encoding the MHV B subclone was mutagenized using primers described in table 1. Plasmids encoding the complete virus genome were digested with restriction enzymes, gel purified, and ligated using T4 ligase at 16°C overnight. The ligation reaction was isopropanol precipitated and *in vitro* RNA transcription was performed using a mMESSAGE mMACHINE Kit (Ambion) according to the following protocol: 40.5°C for 25 min, 37.5°C for 50 min, 40.5°C for 25 min. RNA was electroporated into BHK-R cells, and the electroporated cells were seeded onto DBT cells. The supernatant was harvested 36 hours post-electroporation and plaque assay was performed as described previously (24). RNA was extracted from infected DBT cells at 8 hours post-infection using RNeasy Mini (Qiagen) and cDNA was generated using $RT^2$ First Strand Kit (Qiagen). PCR was performed using replicase primers (Table 1) and purified PCR product was sequenced (amino acids 747-848). AM2 and AM3 were plaque purified and AM2 was subjected to deep sequencing.

**Temperature Shift Experiment.** DBT cells in 6-well plates were infected with 0.1 MOI of wild-type MHV or AM2 at 37°C. At 2, 4, or 6 hours post infection, cells were moved to 39.5°C until 14 hours post-infection when supernatant was harvested and virus titer was determined by plaque assay at 37°C as described previously (25).

**Expression and purification of wild-type and V787S mutant proteins.** The PLP2 sequence was cloned from pCAGGS-MCS-PLP2 (described above) into LIC vector pEV-L8, which is a modified pET-30 plasmid. The expression of wild-type PLP2 and V787S mutant was performed

using *Escherichia coli* strain BL21 (DE3). Cultures were grown in LB medium supplemented with kanamycin (50 ug/ml) at 37°C until the optical density at 600nm (A600) reached 0.6. PLP2 expression was then induced with 0.1mM isopropyl-β-D-thiogalactopyranoside (IPTG) at 25°C for 6h. Wild-type PLP2 was induced at 25°C for 6 h, while the V787S mutant was induced at 18°C overnight. Cells were harvested by centrifugation at 4,690 × g for 20 min at 4°C and stored at -80°C until use. Cell pellets from 1 L culture were then resuspended in 40mL buffer A (25mM Tris pH 7.0, 500mM NaCl, 20mM imidazole, 5mM βME) supplemented with dissolved flakes of lysozyme and DNase, lysed through sonication and centrifuged at 28,880 × g for 30 min (4°C). The supernatant was filtered through a 0.45µm membrane (Millipore) and loaded onto a 5ml Ni HiTrap HP column (GE healthcare) pre-equilibrated with buffer A. Then the column was washed with buffer A supplemented with 5% buffer B (25mM Tris pH 7.0, 500mM NaCl, 500mM imidazole, 5mM βME) until the UV was back to the baseline. The protein was eluted through a gradient of 5%-100% buffer B in 30 column volumes (CV). Fractions were collected and then pooled after enzymatic activity and purity assessment. The n-terminal $(His)_8$-tag was then removed by TEV protease (His-tagged) cleavage by incubating PLP2 and TEV-protease together overnight at 4°C while dialyzing into buffer C (25mM Tris pH 7.0, 100mM NaCl, 10mM βME). Then, free His-tag and TEV protease and uncleaved PLP2 were then separated from cleaved PLP2 by running the sample over a $Ni^{2+}$–charged HiTrap column. The flowthrough was collected and then concentrated using Millipore Micron concentrators to a volume of less than 2 mL. The concentrated sample was loaded onto a Superdex-75 Hiload 26/60 column (GE Healthcare) pre-equilibrated with buffer D (50mM HEPES pH 7.0, 100mM NaCl, 10mM DTT), and eluted at a flow rate of 2 ml/min. Fractions containing active enzyme at high purity, as

judged by SDS-PAGE, were pooled, concentrated and flash-frozen in 2% glycerol using liquid nitrogen for storage at -80°C.

**Temperature inactivation of wild-type and V787S purified protein**. Wild-type PLP2 and the V787S mutant protein were incubated at 25°C for different time periods (0-50 min). At each time point, the specific activity of both enzymes was measured at 25°C using a Synergy Multi-Mode Microplate Reader (BioTek) with 50 µM RLRGG-AMC as the substrate and 3 µM of each enzyme. The assay buffer used contained 50mM HEPES, pH 7.0, 0.1 mg/ml bovine serum albumin (BAS) and 2mM DTT. The experiments were performed in triplicate in a final volume of 100 µl using the 96-well Corning Costar black microplates. Similar experiments were carried out when the enzymes were incubated at 30°C. To analyze the kinetic data, the ratio of the reaction rate at time=t to the rate at time=0 was plotted on a logarithmic scale against incubation time. Kinetic data of the V787S PLP2 incubated at 30°C were fitted to a first-order exponential decay model ($Rate_t/Rate_0 = e^{-kt}$), from which the inactivation rate constant $k_{inact}$ and half-life $t_{1/2}$ were determined. The wild-type data were fit to a line since no significant temperature inactivation was observed.

**Thermal melting temperature ($T_m$) analysis using circular dichroism (CD).** Thermal melting analyses of the wild-type PLP2 and V787S mutant was carried out with a Chirascan circular dichrosim (CD) spectrometer (Applied Photophysics) equipped with a temperature control system (Quantum Northwest Inc.) by monitoring the CD signal at 220nm while increasing the temperature at a step interval of 0.4°C and at a rate 0.5°C/min. Two ml of Protein samples at 1µM in buffer with 0.1M potassium phosphate (pH 7.5) was contained in a 10 mm quartz cell (Starna Cells) with magnetic stirring. Thermal scans were performed in three independent

experiments for both wild-type and V787S mutant MHV PLP2. The melting temperatures ($T_m$) were calculated as the first derivative peak using the program SigmaPlot.

**Generation of bone-marrow derived macrophages and virus infection.** Femur and tibia from 8-week old C57BL/6 female mice were prepared and bone-marrow was isolated, and cultured in IMDM with 10% FCS, 1% pen-strep, 0.1% beta-mercaptoethanol and 5% MCSF obtained from L929-supernatants. Additional medium was added at day 3 post-isolation and cells were seeded at day 6 at a density of $2 * 10^5$ cells/well. The following day, cells were infected with wild-type icMHV A59 and AM2 at an MOI of 1. Medium was changed after two hours and supernatant was harvested at various time points post-infection for titration. Supernatant was titrated on murine fibroblast L929 cells (in MEM containing 10% FCS and 1% pen-strep).

**Mouse studies**. C57BL/6 mice were purchased from the Jackson Laboratory. The mice were maintained, and experiments performed at Loyola University Chicago in accordance with all federal and university guidelines. 4-week old C57BL/6 male mice were anesthetized with ketamine/xylazine prior to intracranial injection with 600 PFU of wild-type icMHV A59 or AM2 mutant. Weight loss and survival were monitored on a daily basis. Mice were sacrificed when they lost 25% of their initial body weight. In other experiments, mice infected with AM2 at 4 weeks of age, and age-matched controls were challenged with 6,000 PFU of wild-type icMHV-A59 at 9 weeks post primary infection. Survival and weight loss were monitored daily. Mice were sacrificed when they lost 25% of the initial body weight. For histology livers were fixed in 4% formalin and paraffin embedded. Sections were stained with hematoxylin and eosin, and analyzed by microscopy.



Journal of Virology

**qRT-PCR analysis**. Brains and livers of 4-week old male mice infected with wild-type icMHV or AM2 were harvested and homogenized at day 3 and 5 post infection and RNA was extracted using RNeasy Mini (Qiagen). Reverse transcription was performed using 2 µg of total RNA and the RT$^2$ First Strand Kit (Qiagen) according to manufacturer's protocol. 1 µl of cDNA was used to set up qRT-PCR reaction according to the manufacturer's protocol using Single Primer Assay for IL-6 (SABiosciences), or replicase primers (table 1). $C_T$ values were normalized to the housekeeping gene (Actin).

## Results

### Identifying the ubiquitin-like domain 2 (Ubl-2) as a modulator of MHV papain-like protease activity

To identify domains and residues within nsp3 that modulate protease activity, we generated a synthetic, codon-optimized parent construct encoding the protease (PLP2, residues 699-1087) in-frame with a V5 epitope tag (Fig. 1A) and introduced a series of mutations into the predicted ubiquitin-like domain 2 (Fig. 1B). Protease activity was evaluated using an established trans-cleavage assay (Fig. 1C). Our goal was to identify a domain that modulated, but did not inactivate protease activity. As a negative control, we generated a PLP2 catalytic mutant (C890A) that was inactive in the trans-cleavage assay. We generated a quadruple mutant (aa 785-788 VDVL/SSSS) and specific single mutants: V785S, D786K, and V787S. We found that substitution of specific residues within the ubiquitin-like domain 2 adjacent to PLP2 consistently affected protease activity and reduced the abundance of cleavage product detected in the trans-cleavage assay when compared to the activity of PLP2-WT (Fig. 1C). To determine the degree to which mutants' protease activity declined we used the recently described GloSensor assay (41).

We found that, consistent with trans-cleavage assay results, all Ubl-2 mutants had decreased protease activity. However, VDVL/SSSS, V785S, and V787S showed the highest defect in protease activity, while D786K showed intermediate phenotype (Fig. 1D). In these experiments similar levels of PLP2 wild-type and mutants were expressed in each sample. These results implicated the Ubl-2 domain as a modulator of viral protease activity in MHV. Further, we determined the deubiquitinating (DUB) activity of the Ubl-2 mutants. We found that quadruple mutant and the single mutants V785S, and V787S had reduced DUB activity compared to wild-type PLP2. In contrast, D786K mutant had similar DUB activity to wild-type PLP2 (Fig. 1E). Therefore, we focused on the Ubl-2 V785S and V787S mutants since these Ubl mutants exhibited the most significant defects in the cell-based assays.

**Ubl-2 mutant virus MHV-AM2 is temperature sensitive**

To determine if substitutions in the Ubl-2 domain affected virus replication, we used reverse genetics (42) to introduce specific mutations into the viral genome and assessed viral replication. Since the phenotype of the mutations in the PLP2 assay (Fig. 1) can be different from the phenotype of the mutant in the context of replicating virus we generated viruses encoding a quadruple mutation VDVL/SSSS, designated MHV-AM1, a single mutation V787S, designated MHV-AM2, and another single mutation V785S, designated MHV-AM3 (Fig. 2A). The presence of the mutations was confirmed by sequencing within the PLP2 domain. MHV-AM1 was highly impaired, generated pinpoint size plaques, and grew to low titer ($1x10^3$ PFU/ml). The low titer and pinpoint plaques generated by AM1 are likely due to the quadruple mutation in PLP2; however, we cannot rule out the possibility that additional mutations outside of PLP2 contribute to this phenotype.



Journal of Virology

In contrast, AM2 and AM3 viruses with single amino acid substitutions within the Ubl-2 domain replicated to titers similar to the parent infectious clone. We found that both AM2 and AM3 viruses generated slightly smaller plaques than those generated by wild-type MHV A59. The small plaque phenotype can be associated with temperature sensitivity, so we evaluated relative plaque size of wild-type and AM2 by performing plaque assays at 39.5°C and 40.5°C. We found that AM2 produced small plaques at 39.5°C (about 50% reduction compared to wild-type), but was unable to generate plaques at 40.5°C (Fig. 2B), consistent with a temperature sensitive defect. AM3 also produced slightly smaller than wild-type plaques but bigger than AM2 plaques at 39.5°C (about 20% reduction compared to wild-type) (data not shown). Because the temperature sensitive phenotype was more severe for AM2 and because V787 is conserved in other betacoronaviruses such as SARS-CoV and MERS-CoV (Fig. 1B), we focused our studies on AM2. We verified the engineered sequence of AM2 by deep sequencing the viral genomic RNA. The 2-nucleotide substitution (gtc to ccc) of V787 was confirmed, and no additional changes were detected (GenBank # in progress).

To determine the replication kinetics of AM2, we infected DBT cells with isogenic wild-type MHV-A59 or AM2 virus at MOI of 0.1. The cells were incubated at 37°C, supernatant was harvested and virus titer was determined by plaque assay. We found that at 37°C, AM2 replicated with similar kinetics to wild-type virus (Fig. 3A). In addition, no replication defect was observed in bone marrow derived macrophages, important primary target cells during MHV infection (Fig. 3B). However, if infected DBT cells were shifted to a higher temperature (39.5°C) there was a progressive reduction in viral titer with increased time at the higher temperature (Fig. 3C). When the cells were incubated at 37°C for 6 hours and then shifted to the higher temperature, the difference between the titers of WT and AM2 was about half a log. In contrast,



Journal of Virology

315 when the infected cells were incubated at 37°C for two hours and then shifted to 39.5°C, the titer
316 of AM2 was two logs lower compared to wild-type virus. Taken together, these data show that
317 AM2 encoding V787S has a temperature sensitive defect in viral replication.

318 **Nsp3-V787S substitution impairs PLP2 thermal stability**

319 To investigate the temperature sensitive phenotype conferred by the V787S substitution,
320 we expressed the wild-type and V787S mutant of MHV PLP2 in *E. coli* and then purified the
321 enzymes to homogeneity using a multi-step chromatography procedure (Fig. 4A). The thermal
322 stability of the wild-type and V787S purified enzymes was then determined at 25°C and at 30°C
323 by measuring the specific activity of the enzymes as a function of incubation time using the
324 peptide-RLRGG-AMC as a substrate. We found that when wild-type and V787S mutant PLP2s
325 were incubated at 25°C, both enzymes were stable over the incubation time course and had
326 similar specific activity (Fig. 4B). The activities in Fig. 4B have been normalized to 100%. In
327 contrast, when wild-type and V787S mutant PLP2s were incubated at a higher temperature
328 (30°C), the specific activity of V787S PLP2 decreased rapidly over time whereas the wild-type
329 protein maintained full activity (Fig. 4B). These results indicate that the V787S enzyme is
330 thermally unstable at 30°C with a half-life of 27.7±1.1 min.

331 To determine the relative structural stability of the purified proteins over a wider
332 temperature range, we performed thermal-denaturation experiments using circular dichroism
333 (CD) analysis to determine the melting temperatures ($T_m$) of each enzyme. Consistent with
334 Figure 4B, the V787S mutant exhibited diminished thermostability (Fig. 4C). The determined
335 melting temperature was 6.8°C lower for the V787S mutant protein than for the wild-type PLP2,
336 suggesting that the V787S mutant PLP2 is less stable and unfolds at a lower temperature than
337 wild-type PLP2. Taken together, our data indicate that the V787S substitution diminished the

overall protein thermal stability resulting in decreased enzymatic activity at elevated temperatures.

**AM2 exhibits reduced pathogenesis and elicits a protective response in mice**

To determine the effect of the Ubl-2 domain mutation on virus pathogenesis, we infected 4-week old male C57B/L6 mice with 600 PFU of wild-type or AM2 virus by intracranial injection. We monitored weight loss over the course of infection and mice were humanely euthanized if they lost greater than 25% of initial body weight. We observed that while 100% of mice infected with wild-type virus succumbed to infection by day 7, all mice infected with AM2 survived the infection (Fig. 5A). We confirmed that the mutation in AM2 was maintained upon mice infection by sequencing within the PLP2 domain of recovered AM2.

We detected similar viral titers in the brains of wild-type or AM2-infected mice at day 3 or day 5 post infection (Fig. 5B). In contrast we found levels of viral replicase and IL-6 were reduced in the livers of AM2 infected mice at day 5 post infection compared to wild-type MHV infected mice (Fig. 5C). There was no difference in CCL2 or IFN-α (data not shown). Furthermore, we analyzed livers for changes in pathology, and observed a reduction in the size of the lesions, hepatocyte necrosis, and inflammation in AM2 infected mice compared to wild-type infected (Fig. 5D). These data indicate that AM2 is attenuated compared to wild-type MHV.

To determine if primary infection with AM2 mutant virus protected mice from challenge with wild-type virus, we infected AM2 immunized and age-matched naïve C57BL/6 mice intracranially with 6000 PFU of wild-type virus at 9 weeks post primary infection. We monitored body weight loss over the course of infection and found that naïve mice lost significantly more weight starting at day 2 post-infection (Fig. 5E). In contrast, AM2 immunized mice did not lose weight and did not exhibit other symptoms of disease upon challenge. 13-week old C57BL/6 are

much more resistant to infection than 4-week mice, so as expected, no wild-type or AM2 infected mice succumbed to the infection. These results indicate that the immunization with AM2 generated a sufficient immune response to protect the mice from subsequent wild-type challenge.

**Discussion**

Modulating viral enzyme activity is a powerful approach for generating attenuated viruses. Coronaviruses encode a very large replicase polyprotein that contains multiple enzymatic activities such as proteases, ADP-ribose-1"-phosphatase (ADRP), methyl-transferase, exonuclease, and RNA-dependent RNA polymerase (see Figure 1). Previous studies have shown that inactivation of the coronavirus papain-like protease by mutagenesis of the required catalytic cysteine residue or inhibition with a protease inhibitor, blocks viral replication (24, 37, 43). These approaches demonstrate the requirement for protease activity, but represent "all or nothing" approaches and do not allow for the study of reduced or impaired protease activity. Here, we describe an approach involving mutation of the domain adjacent to the papain-like protease domain, termed the ubiquitin-like domain (Ubl). Structural studies revealed that this domain is highly conserved in coronaviruses, although the function of this domain is unknown. We found that mutation of the Ubl domain destabilizes the adjacent protease domain, leading to loss of enzymatic activity over time (half-life ~30 min at 30°C). When this mutation is introduced into the virus, the mutant virus replicates efficiently in cell culture at 37°C, but is temperature sensitive and unable to replicate at high temperature (40.5°C). Indeed, we found that this virus is highly attenuated in infected mice but does replicate sufficiently to induce a

protective immune response against wild-type virus. Overall, our studies revealed a new domain that can be exploited for attenuating the pathogenesis of a coronavirus.

Ubl domains have been identified as adjacent to many viral and cellular proteases, particularly the ubiquitin specific proteases (USPs), a family of deubiquitinating enzymes (DUBs) (44). Ubl domains can be present at the C-terminal or N-terminal end of USP catalytic domains, or even can be inserted into the catalytic domain. In addition, USPs may contain one or multiple Ubl domains (45). The Ubl domain of USP14 is required for targeting this cellular DUB to the proteasome. At the proteasome, USP14 removes ubiquitin molecules from proteins that are modified with K48-linked ubiquitin, which serves as a signal for proteosomal degradation (46). Alternatively, the Ubl may regulate function of DUB activity by interacting with other cellular proteins such as GMP synthetase, which enhances the activity of USP7 (47).

Previous studies have shown that the presence of the Ubl domain of SARS-CoV PLpro is necessary for efficient expression and purification of the enzyme (37). To understand the mechanism by which mutations in the Ubl domain of MHV PLP2 affected function, we mapped the mutated residues V785 and V787 into the recently solved crystal structure of MHV PLP2 (Fig. 6) (Chen et al., in preparation). Interestingly, the overall fold of the protease and Ubl-2 domain is conserved between SARS-CoV PLpro and MHV PLP2. Valine 787, which is the focus of this study, is conserved between MHV and highly pathogenic coronaviruses such as SARS-CoV and MERS-CoV (Fig. 1B). Valine 787 resides within a β-sheet that helps to maintain the structure of the Ubl. The side chains of valine 785 and valine 787 participate in the formation of a hydrophobic core of the Ubl, which stabilizes this domain. By mutating valine 787 to serine, we introduced a polar side chain that is energetically unable to pack into the hydrophobic core because of significant desolvation penalties. Therefore, mutation of valine-

406 787 or valine 785 likely disrupts the structure of the Ubl domain thereby leading to the overall
407 destabilization of PLP2 catalytic domain at elevated temperature. As a consequence, the Ubl
408 mutant enzyme has decreased thermal stability that results in a loss of the specific activity of the
409 enzyme over time *in vitro*. Furthermore, the destabilization of Ubl-2-PLP2 has an important
410 impact on virus pathogenesis since we found that MHV-AM2 is attenuated *in vivo*.

411 Interestingly, our studies revealed that the most dramatic reduction in AM2 viral titer in
412 the mice was in the liver, not the brain, which was the site of inoculation. Since MHV-A59 is
413 hepatotropic, it rapidly disseminates to the liver of infected animals (19). The reduction in viral
414 titer in the liver and the decreased size of lesions in the liver (Fig. 5) could be due to either
415 defective viral replication or a more rapid immune response to clear the virus from the liver.
416 Similar phenotype of virus attenuated in the liver but not the brain was described for MHV-A59
417 ns2 mutant (48, 49). In addition, a recent study by Zhang and colleagues showed that an nsp1
418 mutant virus is attenuated in the liver but replicates efficiently in the brain (50). The attenuated
419 phenotype of the nsp1 mutant virus is hypothesized to be due to a more robust immune response
420 to the virus.

421 Recent studies on MERS-CoV showed that PLpro has DUB activity and that this activity
422 is important for antagonism of innate immune response in transfected cells (31, 51). In addition,
423 the arterivirus equine arteritis virus (EAV) PLP DUB activity has been shown to be involved in
424 inhibition of innate immune response in infected cells suggesting that PLP DUB activity might
425 be important for virus pathogenesis *in vivo* (52). Further studies are needed to determine the role
426 of DUB activity in viral replication and pathogenesis and to determine if the attenuation of AM2
427 is primarily immune mediated or due to defective replication and dissemination of the virus.

Coronaviruses encode multiple novel enzymatic activities and previous studies support the concept of modifying/mutating nonstructural proteins to generate attenuated viruses and to identify the role of the protein in virus replication and in causing disease in mice. Mutation of the N-terminal replicase product nsp1 in MHV results in an attenuated infection in mice (53, 54). In addition, mutation of nsp1 in SARS-CoV results in a decrease in antiviral signaling and virus titer in infected cells (55). Mutation of the catalytic residues of the ADP-ribose-1''-phosphatase (ADRP) domain does not diminish virus replication in mice but reduces production of the cytokine IL-6, an important pro-inflammatory molecule (56–58). Reduction in inflammatory response upon infection with ADRP mutant may contribute to decreased liver pathology (56). Genetically inactivating the enzyme ExoN, which has proofreading function, results in a hypermutation phenotype virus that is highly attenuated, even in aged, immunocompromised animals (59). Mutation of the 2'-O-methyl-transferase activity in nsp16 revealed that this activity is required to evade viral mRNA detection by the pattern recognition receptor MDA5 (60, 61). Further, deletion or introduction of an inactivating mutation in nonstructural protein 2 (ns2) in MHV results in the activation of the RNase L pathway, which induces of an antiviral state in liver macrophages (62). All of the aforementioned studies reveal the critical roles of viral nonstructural proteins in virus replication and escape from immune surveillance. Our study reveals a role for the Ubl-2 domain in stabilization of the PLP2 catalytic domain of MHV PLP2 and provides a new target for viral attenuation and potentially for antiviral drug development.

**Acknowledgments**

This work was supported by the NIH grant RO1 AI085089 (to SCB and ADM) and RO1 NS36592 (to SP). ADM is also supported by a grant from the Walther Cancer Foundation. AMM was supported in part by Arthur J. Schmitt Dissertation Fellowship from Loyola University

452 Chicago. EK and VT were supported by the Swiss National Science Foundation (project
453 149784).

## References


1. **Peiris JS, Guan Y, Yuen KY**. 2004. Severe acute respiratory syndrome. Nat. Med. **10**:S88–97.

2. **Zaki AM, van Boheemen S, Bestebroer TM, Osterhaus AD, Fouchier RA**. 2012. Isolation of a novel coronavirus from a man with pneumonia in Saudi Arabia. N. Engl. J. Med. **367**:1814–1820.

3. **WHO.** Available at http://www.who.int/csr/don/03-february-2015-mers/en/

4. **Lau SK, Woo PC, Li KS, Huang Y, Tsoi HW, Wong BH, Wong SS, Leung SY, Chan KH, Yuen KY**. 2005. Severe acute respiratory syndrome coronavirus-like virus in Chinese horseshoe bats. Proc. Natl. Acad. Sci. U. S. A. **102**:14040–14045.

5. **Poon LL, Chu DK, Chan KH, Wong OK, Ellis TM, Leung YH, Lau SK, Woo PC, Suen KY, Yuen KY, Guan Y, Peiris JS**. 2005. Identification of a novel coronavirus in bats. J. Virol. **79**:2001–2009.

6. **Perlman S, Netland J**. 2009. Coronaviruses post-SARS: update on replication and pathogenesis. Nat. Rev. **7**:439–450.

7. **Dominguez SR, O'Shea TJ, Oko LM, Holmes K V**. 2007. Detection of group 1 coronaviruses in bats in North America. Emerg. Infect. Dis. **13**:1295–1300.

8. **Woo PC, Lau SK, Huang Y, Yuen KY**. 2009. Coronavirus diversity, phylogeny and interspecies jumping. Exp. Biol. Med. (Maywood). **234**:1117–1127.

9. **Ge X-Y, Li J-L, Yang X-L, Chmura AA, Zhu G, Epstein JH, Mazet JK, Hu B, Zhang W, Peng C, Zhang Y-J, Luo C-M, Tan B, Wang N, Zhu Y, Crameri G, Zhang S-Y, Wang L-F, Daszak P, Shi Z-L**. 2013. Isolation and characterization of a bat SARS-like coronavirus that uses the ACE2 receptor. Nature **503**:535–8.

10. **Briese T, Mishra N, Jain K, Zalmout IS, Jabado OJ, Karesh WB, Daszak P, Mohammed OB, Alagaili AN, Lipkin WI**. 2014. Middle East Respiratory Syndrome Coronavirus Quasispecies That Include Homologues of Human Isolates Revealed through Whole-Genome Analysis and Virus Cultured from Dromedary Camels in Saudi Arabia. MBio **5**:e01146–14–e01146–14.

11. **Assiri A, McGeer A, Perl TM, Price CS, Al Rabeeah AA, Cummings DA, Alabdullatif ZN, Assad M, Almulhim A, Makhdoom H, Madani H, Alhakeem R, Al-Tawfiq JA, Cotten M, Watson SJ, Kellam P, Zumla AI, Memish ZA, Team the KSAM-CI**. 2013. Hospital Outbreak of Middle East Respiratory Syndrome Coronavirus. N. Engl. J. Med. **369**(5):407-16

12. **Guery B, Poissy J, El Mansouf L, Sejourne C, Ettahar N, Lemaire X, Vuotto F, Goffard A, Behillil S, Enouf V, Caro V, Mailles A, Che D, Manuguerra JC, Mathieu D, Fontanet A, van der Werf S, group the M-C study**. 2013. Clinical features and viral diagnosis of two cases of infection with Middle East Respiratory Syndrome coronavirus: a report of nosocomial transmission. Lancet.

13. **Cotten M, Watson SJ, Zumla AI, Makhdoom HQ, Palser AL, Ong SH, Al Rabeeah AA, Alhakeem RF, Assiri A, Al-Tawfiq JA, Albarrak A, Barry M, Shibl A, Alrabiah FA, Hajjar S, Balkhy HH, Flemban H, Rambaut A, Kellam P, Memish ZA**. 2014. Spread, circulation, and evolution of the Middle East respiratory syndrome coronavirus. MBio **5**:e01062–13–.

14. **Chiu SS, Chan KH, Chu KW, Kwan SW, Guan Y, Poon LL, Peiris JS**. 2005. Human coronavirus NL63 infection and other coronavirus infections in children hospitalized with acute respiratory disease in Hong Kong, China. Clin. Infect. Dis. **40**:1721–1729.

15. **Esper F, Weibel C, Ferguson D, Landry ML, Kahn JS**. 2006. Coronavirus HKU1 infection in the United States. Emerg. Infect. Dis. **12**:775–779.

16. **Van der Hoek L, Pyrc K, Jebbink MF, Vermeulen-Oost W, Berkhout RJ, Wolthers KC, Wertheim-van Dillen PM, Kaandorp J, Spaargaren J, Berkhout B**. 2004. Identification of a new human coronavirus. Nat. Med. **10**:368–373.

17. **Vabret A, Mourez T, Gouarin S, Petitjean J, Freymuth F**. 2003. An outbreak of coronavirus OC43 respiratory infection in Normandy, France. Clin. Infect. Dis. **36**:985–989.

18. **Lau SK, Li KS, Tsang AK, Lam CS, Ahmed S, Chen H, Chan KH, Woo PC, Yuen KY**. Genetic characterization of Betacoronavirus lineage C viruses in bats reveals marked sequence divergence in the spike protein of pipistrellus bat coronavirus HKU5 in Japanese pipistrelle: implications for the origin of the novel Middle East respiratory sy. J Virol.2013 Aug;87(15)8638-50.doi 10.1128/JVI.01055-13.Epub 2013 May 29.

19. **Mielech AM, Chen Y, Mesecar AD, Baker SC**. 2014. Nidovirus papain-like proteases: Multifunctional enzymes with protease, deubiquitinating and deISGylating activities. Virus Res. **194**:184-90

20. **Weiss SR, Leibowitz JL**. 2011. Coronavirus pathogenesis. Adv. Virus Res. **81**:85–164.

21. **Hurst KR, Ye R, Goebel SJ, Jayaraman P, Masters PS**. 2010. An interaction between the nucleocapsid protein and a component of the replicase-transcriptase complex is crucial for the infectivity of coronavirus genomic RNA. J. Virol. **84**:10276–10288.

22. **Hurst KR, Koetzner CA, Masters PS**. 2013. Characterization of a critical interaction between the coronavirus nucleocapsid protein and nonstructural protein 3 of the viral replicase-transcriptase complex. J. Virol. **87**:9159–72.

23. **Ziebuhr J, Thiel V, Gorbalenya AE**. 2001. The autocatalytic release of a putative RNA virus transcription factor from its polyprotein precursor involves two paralogous papain-like proteases that cleave the same peptide bond. J. Biol. Chem. **276**:33220–32.

24. **Graham RL, Denison MR**. 2006. Replication of murine hepatitis virus is regulated by papain-like proteinase 1 processing of nonstructural proteins 1, 2, and 3. J. Virol. **80**:11610–20.

25. **Kanjanahaluethai A, Baker SC**. 2000. Identification of mouse hepatitis virus papain-like proteinase 2 activity. J. Virol. **74**:7911–7921.

26. **Lindner HA, Fotouhi-Ardakani N, Lytvyn V, Lachance P, Sulea T, Menard R**. 2005. The papain-like protease from the severe acute respiratory syndrome coronavirus is a deubiquitinating enzyme. J. Virol. **79**:15199–15208.

27. **Barretto N, Jukneliene D, Ratia K, Chen Z, Mesecar AD, Baker SC**. 2005. The papain-like protease of severe acute respiratory syndrome coronavirus has deubiquitinating activity. J. Virol. **79**:15189–15198.

28. **Clementz MA, Chen Z, Banach BS, Wang Y, Sun L, Ratia K, Baez-Santos YM, Wang J, Takayama J, Ghosh AK, Li K, Mesecar AD, Baker SC**. Deubiquitinating and interferon antagonism activities of coronavirus papain-like proteases. J Virol **84**:4619–4629.

29. **Devaraj SG, Wang N, Chen Z, Tseng M, Barretto N, Lin R, Peters CJ, Tseng CT, Baker SC, Li K**. 2007. Regulation of IRF-3-dependent innate immunity by the papain-like protease domain of the severe acute respiratory syndrome coronavirus. J. Biol. Chem. **282**:32208–32221.

30. **Frieman M, Ratia K, Johnston RE, Mesecar AD, Baric RS**. 2009. Severe acute respiratory syndrome coronavirus papain-like protease ubiquitin-like domain and catalytic domain regulate antagonism of IRF3 and NF-kappaB signaling. J. Virol. **83**:6689–6705.

31. **Mielech AM, Kilianski A, Baez-Santos YM, Mesecar AD, Baker SC**. 2014. MERS-CoV papain-like protease has deISGylating and deubiquitinating activities. Virology **450-451**:64–70.

32. **Xing Y, Chen J, Tu J, Zhang B, Chen X, Shi H, Baker SC, Feng L, Chen Z**. 2013. The papain-like protease of porcine epidemic diarrhea virus negatively regulates type I interferon pathway by acting as a viral deubiquitinase. J. Gen. Virol. **94**:1554–1567.

33. **Yang H, Yang M, Ding Y, Liu Y, Lou Z, Zhou Z, Sun L, Mo L, Ye S, Pang H, Gao GF, Anand K, Bartlam M, Hilgenfeld R, Rao Z**. 2003. The crystal structures of severe acute respiratory syndrome virus main protease and its complex with an inhibitor. Proc. Natl. Acad. Sci. U. S. A. **100**:13190–13195.

34. **Zheng D, Chen G, Guo B, Cheng G, Tang H**. 2008. PLP2, a potent deubiquitinase from murine hepatitis virus, strongly inhibits cellular type I interferon production. Cell Res. **18**:1105–1113.

35. **Frieman M, Basu D, Matthews K, Taylor J, Jones G, Pickles R, Baric R, Engel DA**. 2011. Yeast based small molecule screen for inhibitors of SARS-CoV. PLoS One **6**:e28479.

36. **Clementz MA, Chen Z, Banach BS, Wang Y, Sun L, Ratia K, Baez-Santos YM, Wang J, Takayama J, Ghosh AK, Li K, Mesecar AD, Baker SC**. 2010. Deubiquitinating and interferon antagonism activities of coronavirus papain-like proteases. J. Virol. **84**:4619–4629.

37. **Ratia K, Pegan S, Takayama J, Sleeman K, Coughlin M, Baliji S, Chaudhuri R, Fu W, Prabhakar BS, Johnson ME, Baker SC, Ghosh AK, Mesecar AD**. 2008. A noncovalent class of papain-like protease/deubiquitinase inhibitors blocks SARS virus replication. Proc. Natl. Acad. Sci. U. S. A. **105**:16119–16124.

38. **Ratia K, Saikatendu KS, Santarsiero BD, Barretto N, Baker SC, Stevens RC, Mesecar AD**. 2006. Severe acute respiratory syndrome coronavirus papain-like protease: structure of a viral deubiquitinating enzyme. Proc. Natl. Acad. Sci. U. S. A. **103**:5717–5722.

39. **Lei J, Mesters JR, Drosten C, Anemüller S, Ma Q, Hilgenfeld R**. 2014. Crystal structure of the papain-like protease of MERS coronavirus reveals unusual, potentially druggable active-site features. Antiviral Res.

40. **Yount B, Denison MR, Weiss SR, Baric RS**. 2002. Systematic assembly of a full-length infectious cDNA of mouse hepatitis virus strain A59. J. Virol. **76**:11065–11078.

41. **Kilianski A, Mielech AM, Deng X, Baker SC**. 2013. Assessing activity and inhibition of Middle East respiratory syndrome coronavirus papain-like and 3C-like proteases using luciferase-based biosensors. J. Virol. **87**:11955–62.

42. **Yount B, Curtis KM, Fritz EA, Hensley LE, Jahrling PB, Prentice E, Denison MR, Geisbert TW, Baric RS**. 2003. Reverse genetics with a full-length infectious cDNA of severe acute respiratory syndrome coronavirus. Proc. Natl. Acad. Sci. U. S. A. **100**:12995–13000.

43. **Báez-Santos YM, Barraza SJ, Wilson MW, Agius MP, Mielech AM, Davis NM, Baker SC, Larsen SD, Mesecar AD**. 2014. X-ray Structural and Biological Evaluation of a Series of Potent and Highly Selective Inhibitors of Human Coronavirus Papain-like Proteases. J. Med. Chem. **57**:2393–412.

44. **Zhu X, Ménard R, Sulea T**. 2007. High incidence of ubiquitin-like domains in human ubiquitin-specific proteases. Proteins **69**:1–7.

45. **Faesen AC, Luna-Vargas MPA, Sixma TK**. 2012. The role of UBL domains in ubiquitin-specific proteases. Biochem. Soc. Trans. **40**:539–45.

46. **Hu M, Li P, Song L, Jeffrey PD, Chenova TA, Wilkinson KD, Cohen RE, Shi Y**. 2005. Structure and mechanisms of the proteasome-associated deubiquitinating enzyme USP14. EMBO J. **24**:3747–3756.

47. **Faesen AC, Dirac AMG, Shanmugham A, Ovaa H, Perrakis A, Sixma TK**. 2011. Mechanism of USP7/HAUSP activation by its C-terminal ubiquitin-like domain and allosteric regulation by GMP-synthetase. Mol. Cell **44**:147–59.

48. **Zhao L, Jha BK, Wu A, Elliott R, Ziebuhr J, Gorbalenya AE, Silverman RH, Weiss SR**. Antagonism of the interferon-induced OAS-RNase L pathway by murine coronavirus ns2 protein is required for virus replication and liver pathology. Cell Host Microbe.2012 Jun 14;11(6)607-16.doi 10.1016/j.chom.2012.04.011.

49. **Zhao L, Rose KM, Elliott R, Van Rooijen N, Weiss SR**. 2011. Cell-type-specific type I interferon antagonism influences organ tropism of murine coronavirus. J. Virol. **85**:10058–10068.

50. **Zhang R, Li Y, Cowley TJ, Steinbrenner A, Phillips JM, Yount BL, Baric RS, Weiss SR**. 2015. The nsp1, nsp13, and M proteins contribute to the hepatotropism of murine coronavirus JHM.WU. J. Virol. doi: 10.1128/JVI.03535-14

51. **Bailey-Elkin BA, Knaap RCM, Johnson GG, Dalebout TJ, Ninaber DK, van Kasteren PB, Bredenbeek PJ, Snijder EJ, Kikkert M, Mark BL**. 2014. Crystal Structure of the Middle East Respiratory Syndrome Coronavirus (MERS-CoV) Papain-like Protease Bound to Ubiquitin Facilitates Targeted Disruption of Deubiquitinating Activity to Demonstrate Its Role in Innate Immune Suppression. J. Biol. Chem. **289**:34667–82.

52. **Van Kasteren PB, Bailey-Elkin BA, James TW, Ninaber DK, Beugeling C, Khajehpour M, Snijder EJ, Mark BL, Kikkert M**. 2013. Deubiquitinase function of arterivirus papain-like protease 2 suppresses the innate immune response in infected host cells. Proc. Natl. Acad. Sci. U. S. A. **110**:E838–47.

53. **Lei L, Ying S, Baojun L, Yi Y, Xiang H, Wenli S, Zounan S, Deyin G, Qingyu Z, Jingmei L, Guohui C**. 2013. Attenuation of mouse hepatitis virus by deletion of the LLRKxGxKG region of Nsp1. PLoS One **8**:e61166.

54. **Zust R, Cervantes-Barragan L, Kuri T, Blakqori G, Weber F, Ludewig B, Thiel V**. 2007. Coronavirus non-structural protein 1 is a major pathogenicity factor: implications for the rational design of coronavirus vaccines. PLoS Pathog. **3**:e109.

628 55. **Wathelet MG, Orr M, Frieman MB, Baric RS**. 2007. Severe acute respiratory
629 syndrome coronavirus evades antiviral signaling: role of nsp1 and rational design of an
630 attenuated strain. J. Virol. **81**:11620–33.

631 56. **Eriksson KK, Cervantes-Barragán L, Ludewig B, Thiel V**. 2008. Mouse hepatitis virus
632 liver pathology is dependent on ADP-ribose-1''-phosphatase, a viral function conserved in
633 the alpha-like supergroup. J. Virol. **82**:12325–34.

634 57. **Kuri T, Eriksson KK, Putics A, Züst R, Snijder EJ, Davidson AD, Siddell SG, Thiel**
635 **V, Ziebuhr J, Weber F**. 2011. The ADP-ribose-1''-monophosphatase domains of severe
636 acute respiratory syndrome coronavirus and human coronavirus 229E mediate resistance
637 to antiviral interferon responses. J. Gen. Virol. **92**:1899–905.

638 58. **Fehr AR, Athmer J, Channappanavar R, Phillips JM, Meyerholz DK, Perlman S**.
639 2014. The NSP3 Macrodomain Promotes Virulence in Mice With Coronavirus-induced
640 Encephalitis. J. Virol. **89**:1523-36

641 59. **Graham RL, Becker MM, Eckerle LD, Bolles M, Denison MR, Baric RS**. 2012. A
642 live, impaired-fidelity coronavirus vaccine protects in an aged, immunocompromised
643 mouse model of lethal disease. Nat. Med. **18**:1820–6.

644 60. **Zust R, Cervantes-Barragan L, Habjan M, Maier R, Neuman BW, Ziebuhr J,**
645 **Szretter KJ, Baker SC, Barchet W, Diamond MS, Siddell SG, Ludewig B, Thiel V**.
646 2011. Ribose 2'-O-methylation provides a molecular signature for the distinction of self
647 and non-self mRNA dependent on the RNA sensor Mda5. Nat. Immunol. **12**:137–143.

648 61. **Menachery VD, Yount BL, Josset L, Gralinski LE, Scobey T, Agnihothram S, Katze**
649 **MG, Baric RS**. 2014. Attenuation and Restoration of SARS-CoV Mutant lacking 2' O
650 Methyltransferase Activity. J. Virol. **88**:4251–64.

651 62. **Zhao L, Jha BK, Wu A, Elliott R, Ziebuhr J, Gorbalenya AE, Silverman RH, Weiss**
652 **SR**. 2012. Antagonism of the interferon-induced OAS-RNase L pathway by murine
653 coronavirus ns2 protein is required for virus replication and liver pathology. Cell Host
654 Microbe **11**:607–16.


655

## Figure legends

**Figure 1. MHV-A59 Ubl-2 domain influences papain-like protease activity.** A) Schematic diagram of MHV-A59 ORFs and the Ubl-2 and papain-like protease (PLP) domains within nonstructural protein 3. Expression plasmids PLP2, and the VDVL region (aa 785-788) are indicated. B) Alignment of the predicted ubiquitin-like domains from MHV and MERS-CoV with the structural information from the Ubl domain of SARS-CoV (PDB 2FE8). C) HEK293T cells were transfected with plasmids expressing PLP2 wild-type, PLP2 catalytic mutant CA, VDV Ubl-2 domain mutants in the presence of plasmid expressing the nsp2/3-GFP substrate. At 24 hours post-transfection cells were lysed and analyzed by Western blot. D) PLP2 activity in live-cell assay. HEK293T cells were transfected with pGlo-RLKGG and indicated PLP2 expression plasmids. At 14 hours post infection GloSensor was added and luminesce was assessed hourly. E) HEK293T cells were transfected with Flag-Ub expression plasmid, and wild-type (PLP2-WT) or indicated Ubl-2 mutants. Cells were lysed 24 hours post-transfection and analyzed by Western blot. The figure shows representative data from at least two independent experiments.

**Figure 2. Murine coronavirus AM2 is temperature sensitive for replication.** A) Summary of the characteristics of Ubl mutant viruses recovered by reverse genetics. B) Representative plaques generated by wild-type MHV (WT) or AM2 during incubation at the indicated temperature. DBT cells were inoculated with either WT or AM2, incubated at the indicated temperature and fixed and stained 48 hours post infection. Diameter of each plaque was measured and average diameter and standard deviation indicated for each virus; *$p<0.05$, **$p<0.001$. Figure shows representative data from at least two independent experiments.



Journal of Virology

**Figure 3. Replication kinetics of AM2. .** A) AM2 replication is similar to MHV-WT at 37°C. (A) DBT cells were infected with AM2 or WT at MOI 0.1 or (B) Bone marrow derived macrophages were infected with AM2 or WT at MOI 1. At indicated time points, supernatant was harvested and virus titer determined by plaque assay at 37°C. C) Temperature shift reduces yield of AM2. DBT cells were infected at the MOI 0.1 at 37°C with AM2 or WT. At the indicated time point post infection, cells were moved to 39.5°C until 14 hrs pi when supernatant was harvested and virus titer was determined by plaque assay at 37°C. The error bars represent standard deviation within single experiment. Figure shows representative data from at least two independent experiments.

**Figure 4. Ubl-2 domain is important for MHV PLP2 thermal stability**. A) SDS-PAGE analysis of the final purified PLP2-V787S enzyme. Wild-type and PLP2-V787S mutant PLP2 were expressed and purified from *E. coli* as described in Materials and Methods. B) Temperature-dependent inactivation of wild-type and PLP2-V787S mutant. The specific activity of wild-type (WT) and the V787S mutant PLP2 enzymes were measured after incubation at 25°C and 30°C for different time periods. The specific activities were then normalized to the activity at 0 min ($Rate_t/Rate_0$: rate at time t over initial rate). Kinetic data for the V787S mutant incubated at 30°C were fit to a first-order exponential decay model ($Rate_t/Rate_0 = e^{-kt}$). The calculated inactivation rate constant $k_{inact}$ for the V787S mutant at 30°C is 0.025 ± 0.001 $min^{-1}$ and the half-life ($t_{1/2}$) is 27.7 ± 1.1 min. C) CD melting curves of WT and PLP2-V787S mutant PLP2. The thermal stability of WT and V787S mutant PLP2 was determined by measuring the CD signal at 220 nm as a function of temperature at a step interval of 0.4°C and at a rate 0.5°C/min. Three independent experiments were performed for both WT PLP2 (grey) and V787S mutant (black).

**Figure 5. MHV AM2 is attenuated and generated protective immunity in mice**. A) C57BL/6 mice were infected with 600 pfu WT icMHV or AM2 mutant intracranially and monitored for survival over time (N=7 for each group). B) Virus titers in brains of mice infected with 600 pfu WT icMHV or AM2 were determined at indicated time points p.i. by plaque assay (N=4 to 5). Error bars represent standard deviation. C) RNA levels for viral replicase gene and cellular IL-6 were determined using qRT-PCR in livers at day 5 post infection (N=6). RNA levels were normalized to actin and amount of transcript in WT infected mice was set to 1. Error bars represent SEM. Statistical analysis performed using Student's *t* test. D) Representative samples of hematoxylin and eosin staining of formalin-fixed liver samples at day 5 post infection from mice infected with WT icMHV or AM2 (N=6 for each group, magnification X10). E) C57BL/6 mice immunized with AM2 mutant and naive age-mached controls were challenged with 6000 pfu icMHV intracranially 9 weeks post primary infection. The mice were monitored for body weight loss. Error bars represent SEM.****, $p<0.0001$, two-way ANOVA.

**Figure 6. X-ray structures of the MHV and SARS-CoV Ubl-2 domains**. A superposition of the Ubl-2 domains from MHV PLP2 (blue) and SARS-CoV PLpro (orange, PDB 2FE8) is shown as a stereoview and resulted in RMSD of 0.74 Å. Side chains of MHV Ubl-2 residues V785 and V787, and their corresponding residues in SARS-CoV are shown as sticks.

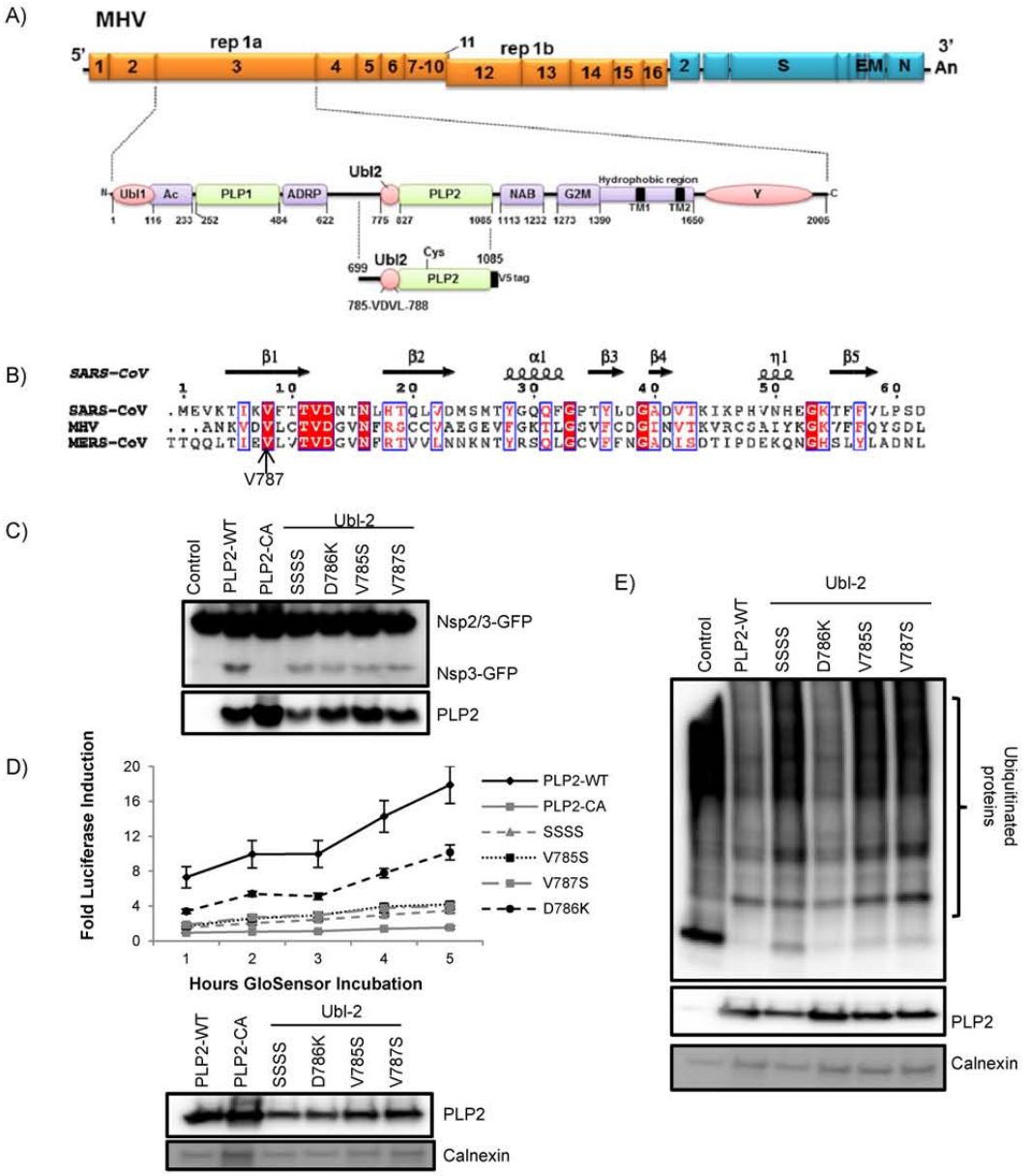


**Figure 1. MHV-A59 Ubl-2 domain influences papain-like protease activity.** A) Schematic diagram of MHV-A59 ORFs and the Ubl-2 and papain-like protease (PLP) domains within nonstructural protein 3. Expression plasmids PLP2, and the VDVL region (aa 785-788) are indicated. B) Alignment of the predicted ubiquitin-like domains from MHV and MERS-CoV with the structural information from the Ubl domain of SARS-CoV (PDB 2FE8). C) HEK293T cells were transfected with plasmids expressing PLP2 wild-type, PLP2 catalytic mutant CA, VDV Ubl-2 domain mutants in the presence of plasmid expressing the nsp2/3-GFP substrate. At 24 hours post-transfection cells were lysed and analyzed by Western blot. D) PLP2 activity in live-cell assay. HEK293T cells were transfected with pGlo-RLKGG and indicated PLP2 expression plasmids. At 14 hours post infection GloSensor was added and luminesce was assessed hourly. E) HEK293T cells were transfected with Flag-Ub expression plasmid, and wild-type (PLP2-WT) or indicated Ubl-2 mutants. Cells were lysed 24 hours post-transfection and analyzed by Western blot. The figure shows representative data from at least two independent experiments.

A)

| Virus | Ubl Mutation | Titer of recovered virus (pfu/ml) | Plaque size |
|---|---|---|---|
| WT | none | $10^7$ | regular |
| AM1 | VDVL/SSSS | $10^3$ | pin point |
| AM2 | V787S | $10^7$ | small |
| AM3 | V785S | $10^7$ | small |

B)

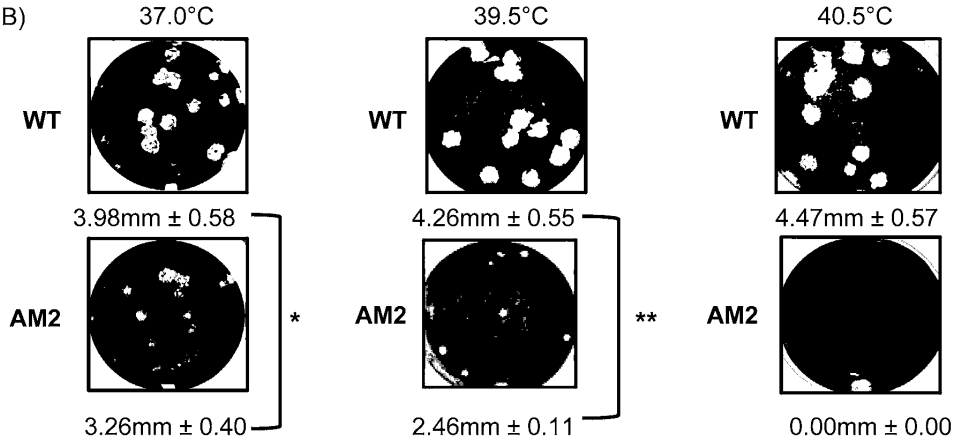


**Figure 2. Murine coronavirus AM2 is temperature sensitive for replication.** A) Summary of the characteristics of Ubl mutant viruses recovered by reverse genetics. B) Representative plaques generated by wild-type MHV (WT) or AM2 during incubation at the indicated temperature. DBT cells were inoculated with either WT or AM2, incubated at the indicated temperature and fixed and stained 48 hours post infection. Diameter of each plaque was measured and average diameter and standard deviation indicated for each virus; *$p<0.05$, **$p<0.001$. Figure shows representative data from at least two independent experiments.

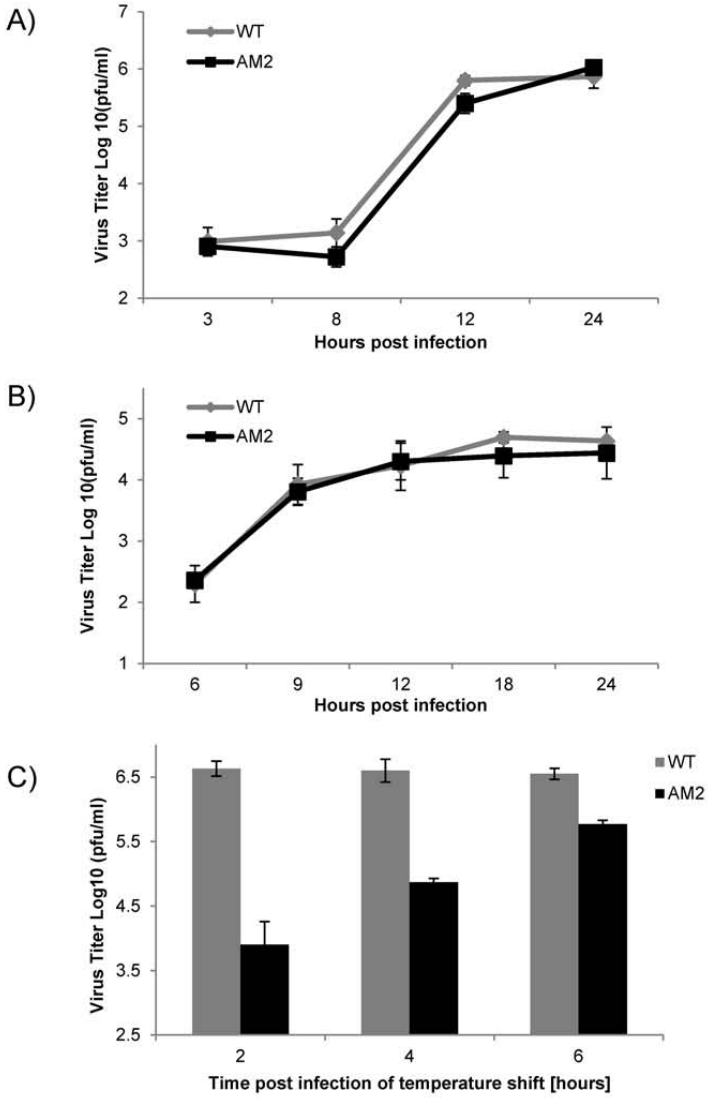


**Figure 3. Replication kinetics of AM2.** A) AM2 replication is similar to MHV-WT at 37°C. (A) DBT cells were infected with AM2 or WT at MOI 0.1 or (B) Bone marrow derived macrophages were infected with AM2 or WT at MOI 1. At indicated time points, supernatant was harvested and virus titer determined by plaque assay at 37°C. C) Temperature shift reduces yield of AM2. DBT cells were infected at the MOI 0.1 at 37°C with AM2 or WT. At the indicated time point post infection, cells were moved to 39.5°C until 14 hrs pi when supernatant was harvested and virus titer was determined by plaque assay at 37°C. The error bars represent standard deviation within single experiment. Figure shows representative data from at least two independent experiments.

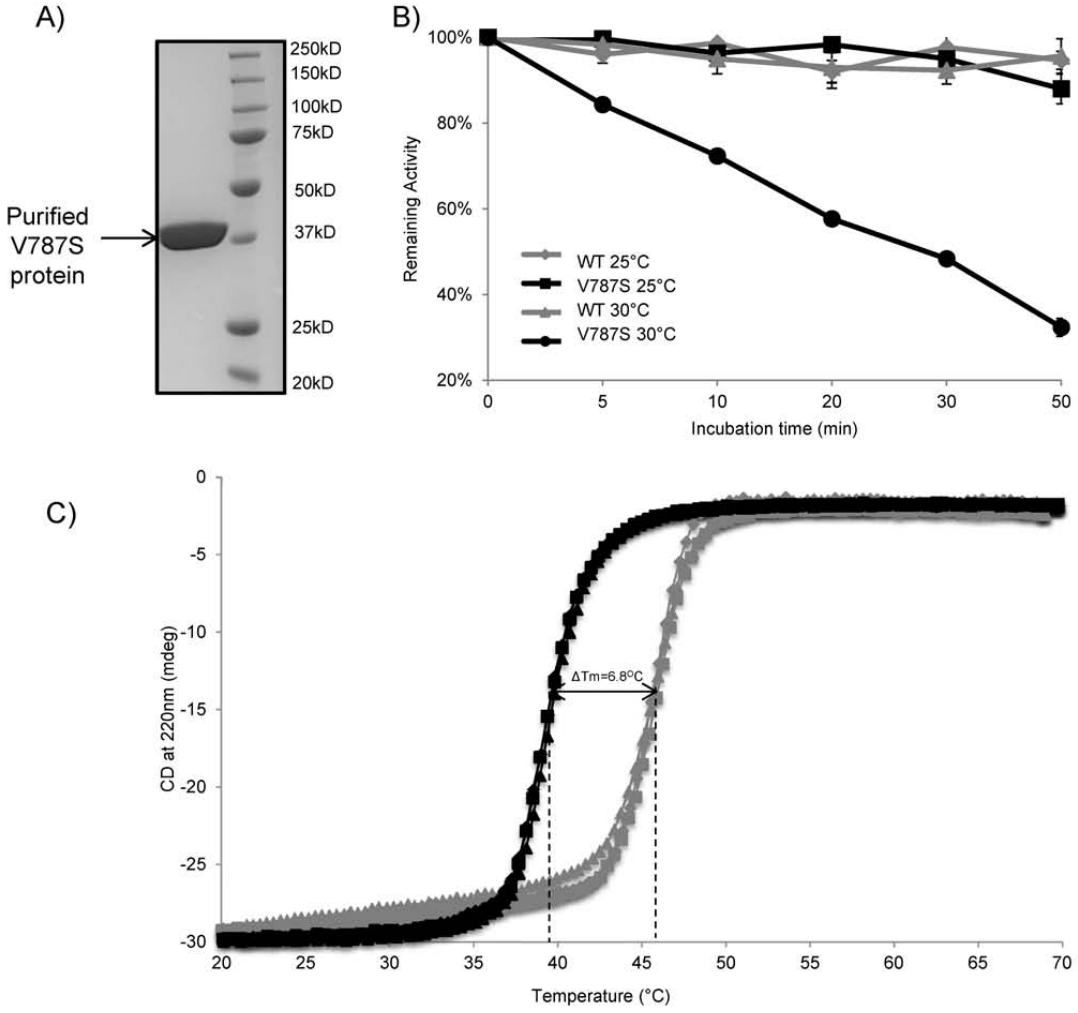


**Figure 4. Ubl-2 domain is important for MHV PLP2 thermal stability**. A) SDS-PAGE analysis of the final purified PLP2-V787S enzyme. Wild-type and PLP2-V787S mutant PLP2 were expressed and purified from *E. coli* as described in Materials and Methods. B) Temperature-dependent inactivation of wild-type and PLP2-V787S mutant. The specific activity of wild-type (WT) and the V787S mutant PLP2 enzymes were measured after incubation at 25°C and 30°C for different time periods. The specific activities were then normalized to the activity at 0 min ($Rate_t/Rate_0$: rate at time t over initial rate). Kinetic data for the V787S mutant incubated at 30°C were fit to a first-order exponential decay model ($Rate_t/Rate_0 = e^{-kt}$). The calculated inactivation rate constant $k_{inact}$ for the V787S mutant at 30°C is 0.025 ± 0.001 $min^{-1}$ and the half-life ($t_{1/2}$) is 27.7 ± 1.1 min. C) CD melting curves of WT and PLP2-V787S mutant PLP2. The thermal stability of WT and V787S mutant PLP2 was determined by measuring the CD signal at 220 nm as a function of temperature at a step interval of 0.4°C and at a rate 0.5°C/min. Three independent experiments were performed for both WT PLP2 (grey) and V787S mutant (black).

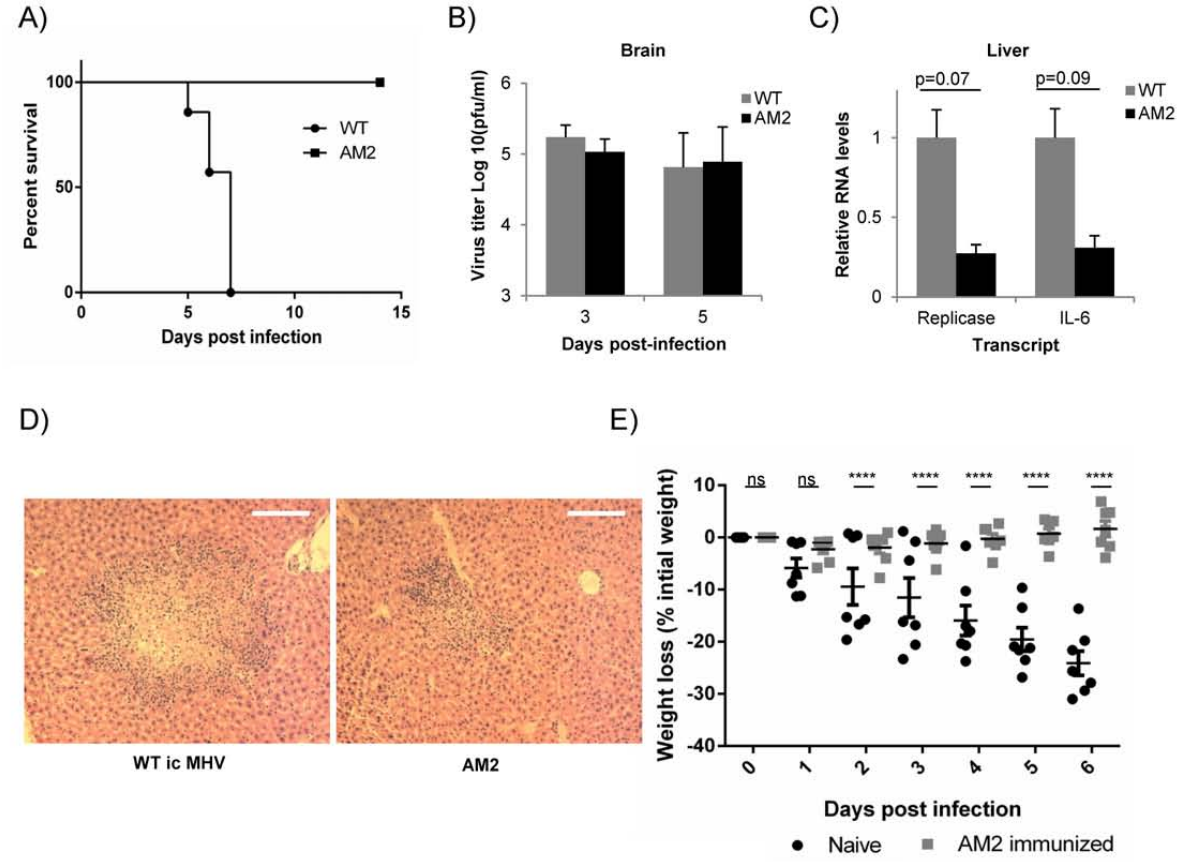


**Figure 5. MHV AM2 is attenuated and generated protective immunity in mice**. A) C57BL/6 mice were infected with 600 pfu WT icMHV or AM2 mutant intracranially and monitored for survival over time (N=7 for each group). B) Virus titers in brains of mice infected with 600 pfu WT icMHV or AM2 were determined at indicated time points p.i. by plaque assay (N=4 to 5). Error bars represent standard deviation. C) RNA levels for viral replicase gene and cellular IL-6 were determined using qRT-PCR in livers at day 5 post infection (N=6). RNA levels were normalized to actin and amount of transcript in WT infected mice was set to 1. Error bars represent SEM. Statistical analysis performed using Student's *t* test. D) Representative samples of hematoxylin and eosin staining of formalin-fixed liver samples at day 5 post infection from mice infected with WT icMHV or AM2 (N=6 for each group, magnification X10). E) C57BL/6 mice immunized with AM2 mutant and naive age-mached controls were challenged with 6000 pfu icMHV intracranially 9 weeks post primary infection. The mice were monitored for body weight loss. Error bars represent SEM.****, p<0.0001, two-way ANOVA.

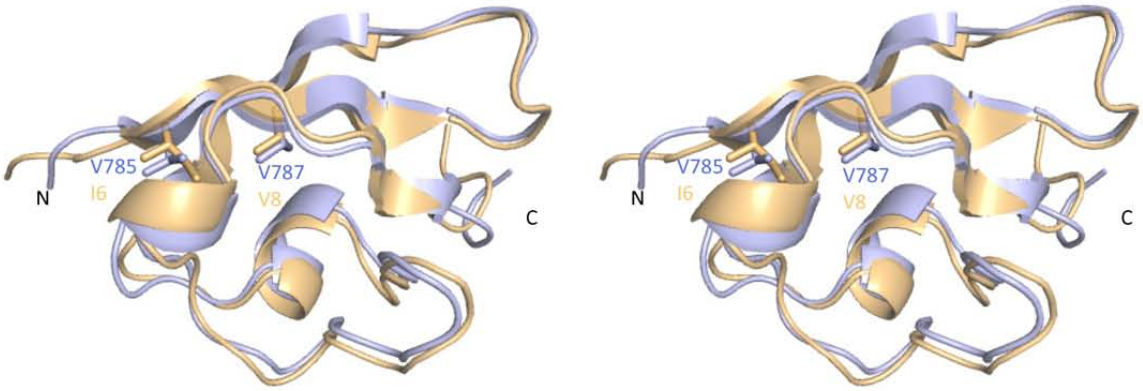


**Figure 6. X-ray structures of the MHV and SARS-CoV Ubl-2 domains.** A superposition of the Ubl-2 domains from MHV PLP2 (blue) and SARS-CoV PLpro (orange, PDB 2FE8) is shown as a stereoview and resulted in RMSD of 0.74 Å. Side chains of MHV Ubl-2 residues V785 and V787, and their corresponding residues in SARS-CoV are shown as sticks.

Table 1. Primers

| | Forward Primer | Reverse Primer |
|---|---|---|
| PLP2-CA | 5' G TCA AAC AAC AAC GCC TAC ATC AAC G | 5' CGT TGA TGT AGG CGT TGT TGT TTG AC |
| SSSS | 5' GGC CAA TAA GAG CAG TAG TAG TTG CAC CGT CGA CGG | 5' CCG TCG ACG GTG CAA CTA CTA CTG CTC TTA TTG GCC |
| V785S | 5' GGC CAA TAA G AGT GAT GTG CTG TG CAC CGT CGA CG | 5' CGT CGA CGG TGC ACA GCA CAT CAC TCT TAT TGG CC |
| D786K | 5' GGC CAA TAA G GTC AAA GTG CTG TG CAC CGT CGA CG | 5' CGT CGA CGG TGC ACA GCA CTT TGA CCT TAT TGG CC |
| V787S | 5' GGC CAA TAA G GTC GAT TCG CTG TG CAC CGT CGA CG | 5' CGT CGA CGG TGC ACA GCG AAT CGA CCT TAT TGG CC |
| AM1 | 5' CTC GCT AAT AAG AGT TCG TCC TCG TGT ACT GTT GAT GG | 5' CCA TCA ACA GTA CAC GAG GAC GAA CTC TTA TTA GCG AG |
| AM2 | 5' CTC GCT AAT AAG GTT GAT TCC TTG TGT ACT GTT GAT GG | 5' CCA TCA ACA GTA CAC AAG GAA TCA ACC TTA TTA GCG AG |
| AM3 | 5' CTC GCT AAT AAG TCT GAT GTC TTG TGT ACT GTT GAT GG | 5' CCA TCA ACA GTA CAC AAG ACA TCA GAC TTA TTA GCG AG |
| Replicase | 5' GAA TGC CCG GGC GGG ATT TTT GTA TCC | 5' CCA CAA GAT CTG CCT CGG ACA AAT C |